Energy Transformation in the Fracture Process of Concrete

By

Kiyoshi OKADA*, Wataru KOYANAGI* and Keitetsu ROKUGO*

(Received March 31, 1977)

Abstract

Fracture process of concrete in compression and in flexure was investigated in terms of an energy transfer concept.

Reversible and irreversible energies in the fracture process were calculated from the load-deformation diagrams. The reversible strain energy of the concrete specimens becomes largest around the maximum load. Two types of irreversible dissipating energies, E_{crac} consumed by crack formation and E_{fric} consumed by viscous friction, under various water contents were calculated. When a concrete specimen is loaded repeatedly in high compression, the energy E_{crac}, consumed by the crack formation in the first load repetition, becomes larger as the water contents of the concrete decrease. Crack growth from a notch in a beam under a flexural load was closely related with the irreversible dissipating energy. The crack growth from a notch is proportional to the energy dissipation in the beam. Therefore, the dissipating energy calculated from the load-deformation diagrams would be used as an index of damage due to the crack formation in concrete. Propagating cracks in a beam were located by detecting the acoustic emissions.

1. Introduction

The fracture process of concrete as a composite material is a process of the growth of internal cracks.

The stress and strain distributions in concrete under a load are far from being uniform even from a submacro-structural view point. Therefore, in order to clarify the fracture process of concrete specimens as systems, the approach in terms of energy, calculated from the load and deformation of the systems, is more favorable than that in terms of stress and strain. Recently, the fracture process of concrete or rock is being studied in the terms of energy by using stiff testing machines[1-5].

As shown in Fig. 1, energy E_t applied to a concrete specimen by an external load is divided into two parts. One is the reversible strain energy

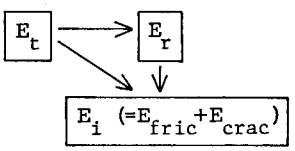

Fig. 1. Energy change in fracture process of concrete.

* Department of Civil Engineering

E_r and the other is the irreversible dissipating energy E_i. The energy E_i may be assumed to consist of two components: E_{crac} consumed by crack formation and E_{fric} consumed by viscous friction. The reversible and irreversible energies are calculated from the load-deformation diagrams.

In this paper, the fracture process of concrete in compression and in flexure is investigated in terms of the energy transfer concept. For the fracture process of concrete under an uniaxial compressive load, the energy transformation affected by the loading rate and the amount of water content of concrete is investigated. The two types of dissipating energies, E_{fric} and E_{crac}, under various water contents, were also calculated. For the fracture process of concrete under a flexural load, the crack growth from a notch is closely related with the dissipating energy. Propagating cracks in a specimen were located by detecting the acoustic emissions from the specimen.

2. Experimental Procedures

2-1 Specimens

Cylindrical specimens $\phi 10 \times 20$ cm were used in the compression tests. Beams $4.7 \times 10 \times 39$ cm with a notch as shown in Fig. 2, or without a notch were used in the flexural tests.

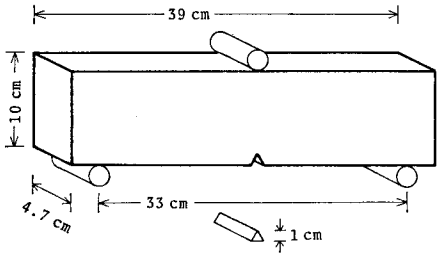

Fig. 2. Beam specimen with a notch.

Three kinds of concrete with different mix proportions, C-1, B-1 and B-2, were cast. Mix proportions, measured slumps and loading ages of the concrete specimens are shown in Table 1.

Techniques of energy calculation and the effect of loading rates on the energies were investigated by compression tests on concrete specimens with the mix proportion C-1. The specimens were cured in 20°C water for three weeks after being cast, and then sored in the laboratory until the testing age.

The effect of water content in concrete in the process under a compressive load was investigated on specimens of the same mix proportion C-1. The specimens were cured in 20°C water for three weeks and then stored in three different storage

Table 1. Mix proportions.

Kinds of mix		C-1	B-1	B-2
Water cement ratio (%)		63	49	65
Mix proportion (Kg/m^3)	Water	216	200	162
	Cement	343	410	250
	Fine agg.	698	658	788
	Coarse agg.	1063	1082	1186
Water reducing agent, cement × (%)		—	1.0	—
Measured slump (cm)		5	5	9
Age at loadings (days)		43±3	17±3	46±3

Table 2. Storage conditions and loss of water.

Group	C-174	C-119	C-0
Relative humidity (%)	25	80	(in water)
Temperature (°C)	70	70	70
Loss of water (g)	174	119	0

conditions for a period of 19 days before loading, to vary the water content in concrete. The storage conditions and the loss of water from the cylindrical specimens during the storage are shown in Table 2.

The relation between the crack growth and energy dissipation under a flexural load was investigated in tests of concrete beams with the mix proportions B-1 and B-2. In particular, the effect of water content in concrete on the energy dissipation was investigated on dry or wet beams with the mix proportion B-2. The location of crack sources was detected on a dry beam with the mix proportion B-2. Wet beams were cured in 20°C water until the loading age, and dry beams were cured in the water for 12 days and then stored in the laboratory until the loading age.

Ordinary portland cement (except for the mix propotion B-1, where high early strength portland cement was used), fine and uniform graded sand (Toyoura standard sand: specific gravity $\rho_S = 2.63$ and size of about 0.1–0.3 mm) and crushed coarse aggregate ($\rho_G = 2.64$) were used in casting three kinds of concrete. The maximum size of the aggregate was 15 mm.

2-2 Testing apparatus

A stiff testing machine automatically controlled with a servo-controller was used for the compression tests and also for the flexural tests of concrete beams with

the mix proportion B-1. Beams with the mix proportion B-2 were tested on a testing machine, in which a sufficiently high stiffness was obtained by connecting the two lateral frames of the machine with a high-strength steel rod (ϕ 32 mm), as shown in Fig. 3.

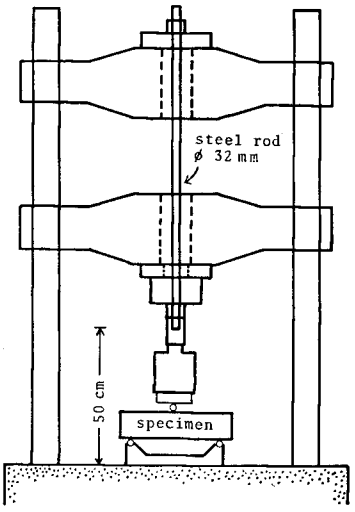

Fig. 3. Testing machine for flexure.

All beams were tested at the center-point loading with an overall span of 33 cm. The deflection of the beam was measured by a straingaged cantilever attached to the beam. The compressive deformation of the cylindrical specimen was measured by three differential transformers attached to the specimen. Load-deformation diagrams were recorded by an $X-Y$ recorder. Complete load-deformation diagrams including the falling branch were obtained under constant deformation rates; mainly 0.4 mm/min. (strain rate; 34×10^{-6}/sec.) in the compression tests of the cylindrical specimens and 0.5–0.05 mm/min. in the flexural tests of the beams. On the other hand, during the repeated compressive loading, the load rate was kept constant; 24 t/min. (stress rate; 5 kg/cm^2/sec.).

2-3 Detection of acoustic emission

Acoustic emissions with a frequency ranging from 20 to 300 KHz were detected from one dry beam by four pickups (ϕ 7 mm) attached to the beam as shown in Fig. 4 and recorded as shown in Fig. 5. Differences D_1, D_2, D_3, of distances between a crack source and each pickup were calculated by the differences of the arrival times of the acoustic emission multiplied by the velocity of the waves in the

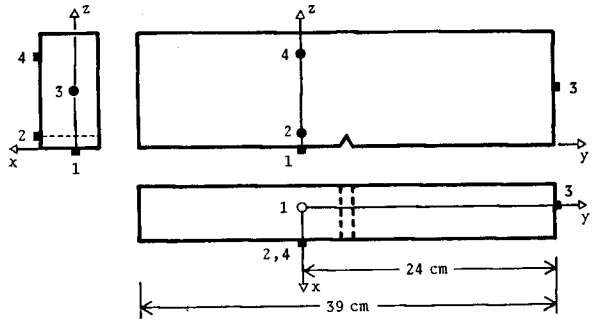

Fig. 4. Location of pickups.

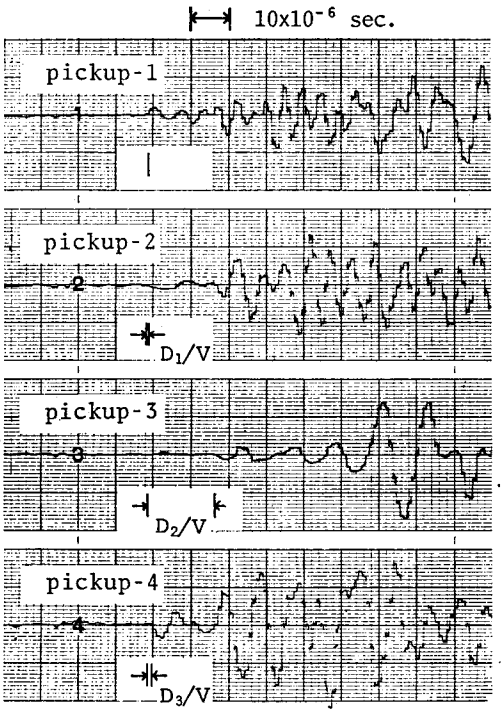

Fig. 5. Example of recording data of acoustic emission.

concrete beam. The co-ordinates (x, y, z) of the crack source can be obtained by solving the following equations.

$$\sqrt{(x-a_i)^2+(y-b_i)^2+(z-c_i)^2}-\sqrt{x^2+y^2+z^2}=D_i \qquad (i=1, 2, 3)$$

where (a_i, b_i, c_i) are co-ordinates of the pickups as shown in Fig. 4.

3. Results and Discussions

3-1 Calculation of the energies

The applied energy E_t and its transformed components E_r and E_i, described above, were calculated by the measuring areas in the load-deformation diagrams. In Fig. 6, E_r and E_i are represented by areas PQR and OPR, respectively. Two types of load-deformation diagrams were adopted for the calculation. The diagram of type 1 was obtained under a single process of loading and unloading. The diagram of type 2 was obtained under the repeated loading and unloading as shown in Fig. 7.

Fig. 8 shows the relation between the deformation D and the applied and reversible energies E_t and E_r, respectively, calculated from the diagrams of type 1.

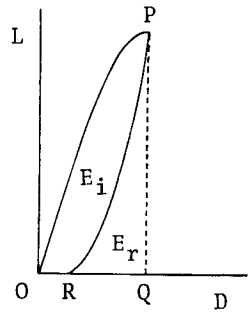

Fig. 6. Calculation of energies.

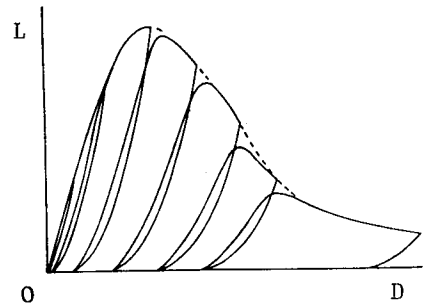

Fig. 7. Load-deformation diagram of type 2.

In Fig. 8, these energies E_t and E_r are normalized by E_{tc} which is the value of E_c at the maximum load, and the deformation D is also normalized by D_c which is the deformation corresponding to the maximum load. The same normalization is performed in Fig. 9. Such curves as shown in Fig. 8 are referred to as energy-deformation relations hereafter. Fig. 9 shows the energy-deformation relations calculated from the diagrams of type 2. Figs. 8 and 9 show that the reversible strain energy under compression is largest at the maximum load ($D/D_c=1$). The energy-deformation relations in Figs. 8 and 9, which are obtained from the two types of load-deformation diagrams, are almost identical to each other. Consequently, energy-deformation relations can be easily obtained from the diagrams of type 2 instead of from the diagrams of type 1, each corresponding to many deformation levels.

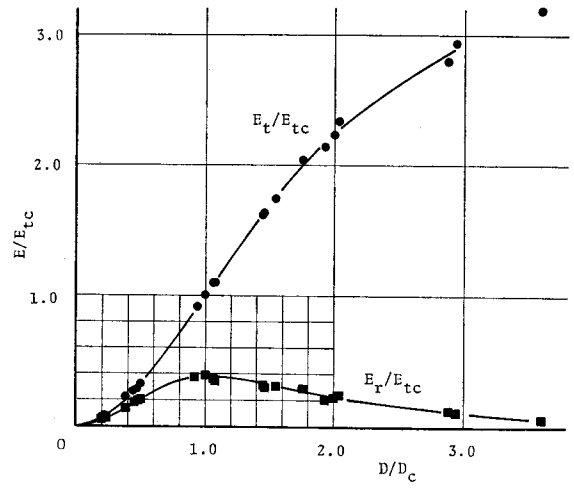

Fig. 8. Energy-deformation relations calculated from diagrams of type 1.

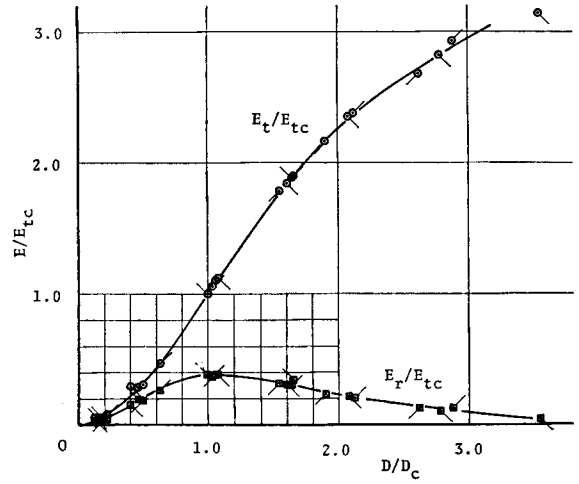

Fig. 9. Energy-deformation relations calculated from diagrams of type 2.

3-2 Effect of the rate of loading

The amount of various energy components at the maximum load is considered to express the trend of energy change during the fracture process of concrete. Hereafter, E_{tc}, E_{rc} and E_{ic} are used to represent the energies E_t, E_r and E_i at the maximum load, respectively. The compressive strength of concrete, the maximum load and energy ratios E_{rc}/E_{tc}, E_{ic}/E_{tc}, E_{rc}/E_{ic} of cylindrical specimens under three kinds of deformation rates are shown in Table 3. These values are the

Table 3. Effect of loading rate on energy components.

Deformation rate (mm/sec.)	2	0.4	0.08
Strain rate ($\times 10^{-6}$/sec.)	170	34	6.8
Max. load (t)	29.1	26.8	26.4
Comp. strength σ_c (kg/cm^2)	371	341	336
E_{rc}/E_{tc}	0.39	0.37	0.36
E_{ic}/E_{tc}	0.61	0.63	0.64
E_{rc}/E_{ic}	0.65	0.58	0.56

averages of each four specimens. As the deformation rate increases, the compressive strength σ_c and the energy ratio E_{rc}/E_{ic} increase. The results of these energy changes show that the increase in compressive strength under a high deformation rate is caused by the decrease of time-dependent deformation.

3-3 Effect of the water content of concrete

The energy ratios at the maximum load of three groups of concrete having different water contents are shown in Table 4. The lower the water content, the larger the energy ratio E_{rc}/E_{ic}. It is shown obviously that the increase in compressive strength due to a decreased water content is caused by the increase of internal bonding energy and frictional resistance.

Table 4. Effect of water content on energy components.

Group	C-174	C-119	C-0
Max. load (t)	27.6	27.6	26.5
Comp. strength σ_c (kg/cm^2)	352	352	338
E_{rc}/E_{tc}	0.49	0.48	0.44
E_{ic}/E_{tc}	0.51	0.52	0.56
E_{rc}/E_{ic}	0.95	0.91	0.79

Specimens of mix proportion C-1 were subjected to the repeated or sustained load, each lower than the maximum load, and the loadings were controlled by compressive strain. The maximum stress σ_{max} adopted in the loading corresponds to the predetermined strain ε_1 in the virginal stress-strain curve of the concrete. The number of load repetitions or the duration of sustained loadings, each required to attain the higher strain level $\varepsilon_2(=\varepsilon_1+200\times10^{-6})$ increases as the water content decreases, as shown in Table 5. The rate of increase of the duration is larger than that of the number of repetitions.

Table 5. Number and duration of loadings.

Group	C-174	C-119	C-0
Strain ε_1 ($\times10^{-6}$)	1225	1175	1185
Max. strength σ_{max} (kg/cm^2)	289	291	281
Stress ratio σ_{max}/σ_c	0.82	0.83	0.83
Number of load repetition	12.6	8.2	4.3
Duration of sustained loading (min.)	23.5	6.2	1.4

The relation between the dissipating energy E_i for a cylindrical specimen of volume (1570 cm^3) and the number of load repetitions is shown in Table 6. The dissipating energy E_i shows a maximum value at the first repetition and becomes almost constant after a few repetitions. By means of acoustic emissions and direct observation of the internal cracking, it is confirmed that the greater part of the

internal crack under repeated loading occurs during the first repetition. And the constant dissipating energy described above is considered to be E_{fric}. Therefore, the dissipating energy E_i at the first repetition (E_{i1}) can be divided into two components, E_{crac} and E_{fric}. Assuming that E_{fric} is equal to E_i at the 8th repetition as shown in Table 6, E_{crac} and E_{fric} obtained at the first repetition of the repeated loading are calculated and shown in Table 7. As the water content in concrete decreases, E_{crac} increases and E_{fric} decreases.

Table 6. Load repetition and dissipating energy.

Group		C-174	C-119	C-0
E_i (kg·cm)	1 st	122	121	128
	2 nd	43	43	58
	4 th	35	35	50
	8 th	34	33	50
	16 th	31	33	—

Table 7. Components of dissipating energy at the first loading.

Group	C-174	C-119	C-0
E_{crac} (kg·cm)	88	88	78
E_{fric} (kg·cm)	34	33	50
E_i (kg·cm)	122	121	128
E_{fric}/E_{crac}	0.38	0.37	0.63

3-4 Crack growth and energy dissipation

Load-deflection curves of the wet beams of B-1, B-2 and the dry beams of B-2 are shown in Figs. 10, 11 and 12, respectively. In these figures one load-deformation diagram was obtained from one beam. From these load-deformation diagrams the dissipating energy during the loading was calculated. The crack

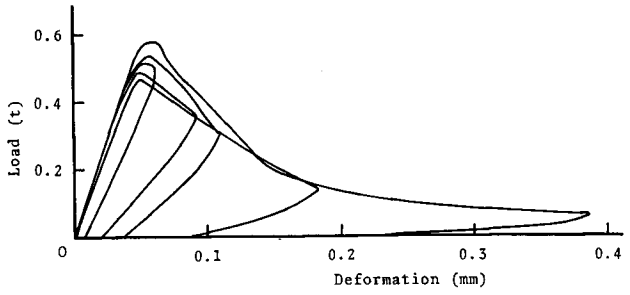

Fig. 10. Load-deformation diagrams. (wet beams of B-1)

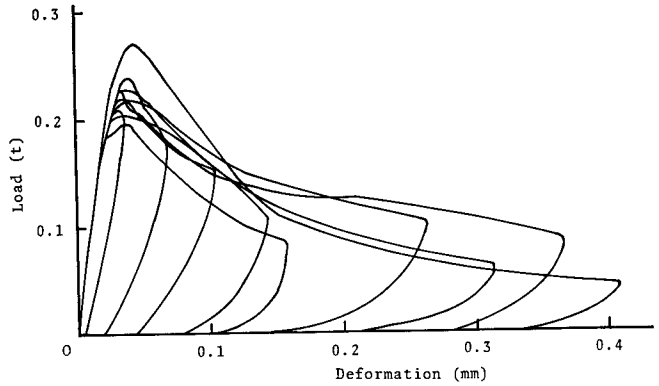

Fig. 11. Load-deformation diagrams. (wet beams of B-2)

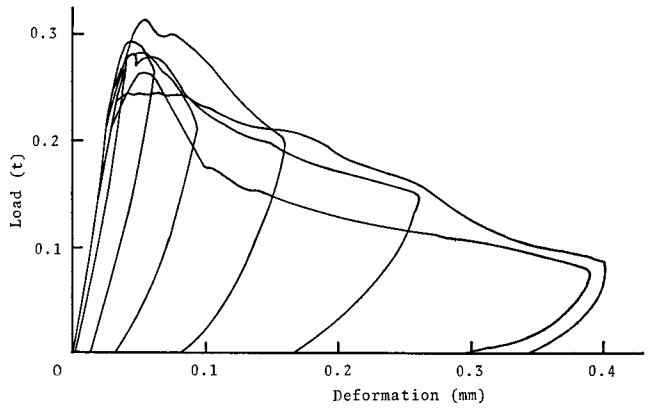

Fig. 12. Load-deformation diagrams. (dry beams of B-2)

surface from a notch in the beam was, after being tested, dyed a dark blackish brown by a solution of polycyclic sulfonate type compounds, which is a kind of chemical admixture for concrete to be used as a powerful water reducing agent. After the drying of the dyes, the beams were again loaded and broken down into two parts as shown in Fig. 13. The average depth of the dyed crack surface from a notch after the first loading was measured for each beam. The relation between the crack depth measured from the dyed surface and the dissipated energy measured from the load-deformation diagrams is shown in Fig. 14 for the wet or dry beams. It can be seen from Fig. 14 that the crack growth from a notch under a flexural load is proportional to the energy dissipation in the beam. Thus it may be concluded that the dissipating energy calculated from the load-deformation diagrams would be used as an index of damage due to crack formation in concrete.

The strength of concrete of B-1 and B-2 and the maximum load of the con-

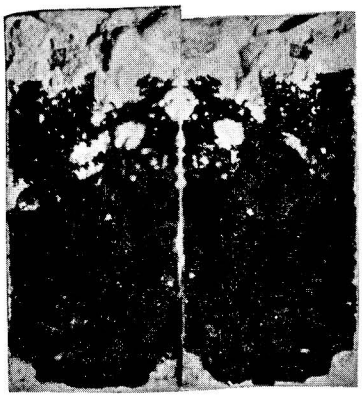

Fig. 13. Dyed cracked surface.

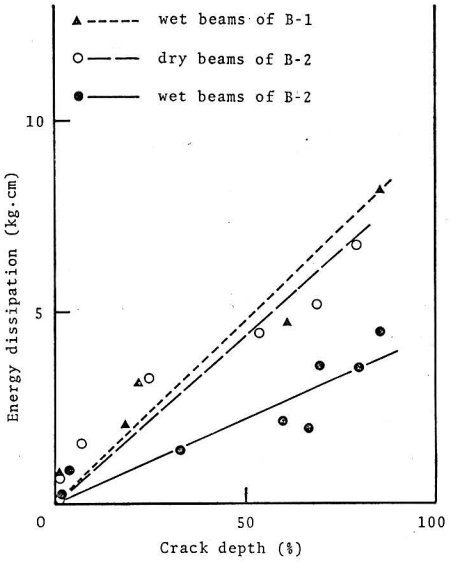

Fig. 14. Crack depth and energy dissipation.

crete specimens under a compressive or a flexural load are shown in Table 8. The total dissipated energy for the complete failure of specimens of B-1 and B-2 under a compressive or a flexural load is roughly estimated from each load-deformation diagram and shown in Table 9. The modulus of rupture of the dry beam of B-2

Table 8. Strength of concrete of B-1 and B-2.

Kinds of concrete		B-1 wet	B-2	
			wet	dry
Max. comp. load (t)		46.4	10.6	12.7
Comp. strength (kg/cm^2)		591	135	162
Max. flex. load (t)	without notch	0.635	0.235	—
	with notch	0.522	0.215	0.264
Modulus of ruptrue (kg/cm^2)	without notch	82.6	31.9	—
	with notch	67.9	28.0	34.3

Table 9. Total dissipating energy for complete failure. (kg·cm)

Kinds of concrete	B-1 wet	B-2	
		wet	dry
In compression	1.8×10^3	1.4×10^3	—
In flexure	9.5	4.5	9.0

is about 1.2 times as large as that of the wet beams of the same mix proportion. However, the energy dissipation of the dry beams is 2 times as large as that of the wet beams.

3-5 Location of crack sources in the beam

Crack sources calculated from 78 values out of 150 measurements of acoustic emission detected by four pickups as explained in section 2–3 were located inside the beam and shown in Fig. 15. The order of the occurrence of acoustic emissions is shown in Fig. 16 as points plotted on the load-deformation diagram. The relation between the occurrence of acoustic emission and the depth of the crack source is shown in Fig. 17, the abscissa corresponding to the deformation in Fig. 16. The frequency of acoustic emissions before the maximum flexural load is lower than that after the maximum load. The acoustic emissions before the maximum load were mainly caused by the local fracture near the center loading point. There can be seen a tendency in Fig. 17, that the later the occurrence of acoustic emissions, the larger the depth of the crack sources.

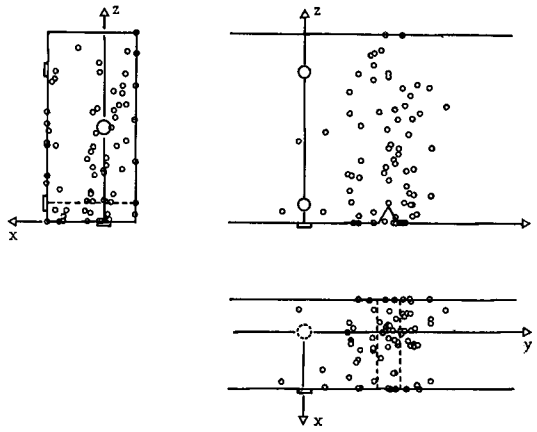

Fig. 15. Located crack sources in the beam.

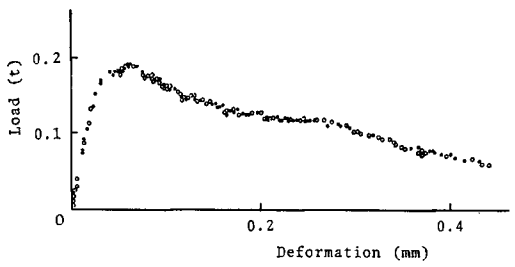

Fig. 16. Order of the occurrence of acoustic emissions.

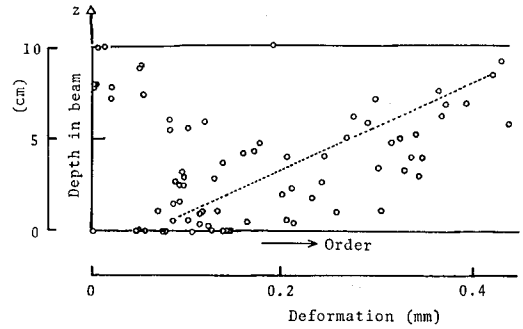

Fig. 17. Order of acoustic emission and depth of the source.

3-6 Energy versus deformation relations of beams

Fig. 18 shows the energy-deformation relations of wet beams with the mix proportion B-2, as an example, calculated from the diagrams of type 2. Not only under a compressive load but also under a flexural load, the elastic strain energy of a specimen is largest around the maximum load.

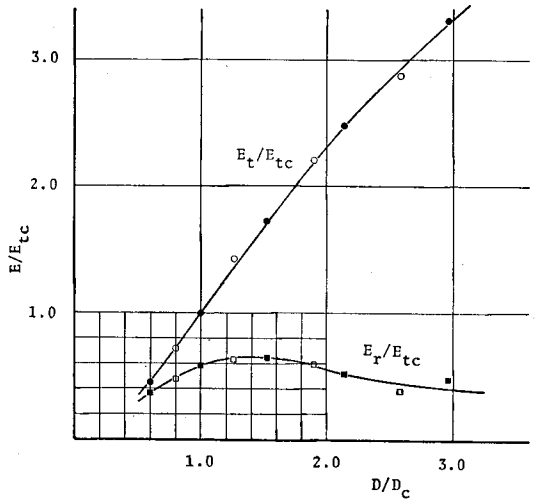

Fig. 18. Energy-deformation relations of wet beams of B-2.

4. Conclusions

The fracture process of concrete in compression and in flexure was investigated in terms of the energy transfer concent.

Following conclusions were obtained.

(1) In the fracture process of a concrete specimen under a compressive load, the reversible strain energy of the specimen is largest at the maximum load. Also

under a flexural load the reversible strain energy of a beam is largest around the maximum load.

(2) It is explained by the energy transfer concept, that the increase in compressive strength under a high loading rate is caused by the decrease of time-dependent deformation, and that the increase in compressive strength due to the decreased water content is cuased by the increase of internal bond energy and frictional resistance.

(3) The effects of the water content in concrete on the fracture process are fairly different between in fatigue and in creep fracture. Dried concrete is more deformable under a repeated loading than under a sustained loading.

(4) When concrete specimens are loaded repeatedly in high compression, the energy E_{crac}, consumed by the crack formation in the first repetition, becomes larger as the water content of the concrete decreases.

(5) The crack growth from a notch in beams under a flexural load is proportional to the energy dissipation in the beams. Therefore, the dissipating energy calculated from the load-deformation diagrams would be used as an index of damage due to the crack formation in concrete.

(6) Propagating cracks in a beam were located by detecting the acoustic emissions. There is a tendency that the later the occurernce of acoustic emissions, the larger the depth of a crack source.

5. Acknowledgements

The authors are indebted to Mr. M. Ootsu for the location of crack sources by detecting the acoustic emissions, and wish to thank Mr. K. Ootani for experiments of the flexural tests.

References

1) Y. Nishimatsu, K. Matsuki and S. Koizumi: J. Soc. Mat. Sci. Jap., **23**, 374 (1974–5).
2) K. Okada, W. Koyanagi and K. Rokugo: Proc. 2nd Int. Conf. Mech. Behav. Mat., 1358, Boston (1976–8).
3) K. Okada, W. Koyanagi and K. Rokugo: Proc. Jap. Soc. Civ. Eng., No. 248, 129 (1976–4).
4) D.C. Spooner and J.W. Dougill: Mag. Con. Res., **27**, No. 92, 151 (1975–9).
5) D.C. Spooner, C.D. Pomeroy and J.W. Dougill: Mag. Con. Res., **28**, No. 94, 21 (1976–3).